Identification of collagen fibrils in cross sections of bone by electron energy loss spectroscopy (EELS)

Bryan E.J. Lee[1], Lucy Luo[2], Kathryn Grandfield[1,3], Carmen M. Andrei[4] and Henry P. Schwarcz[4,5*]

1. School of Biomedical Engineering, McMaster University, Hamilton, ON, L8S 4L7, Canada

2. Bachelor of Health Sciences (BHSc) Program, McMaster University, Hamilton, ON, L8S4L8, Canada

3. Dept. of Materials Science and Engineering, McMaster University, Hamilton, ON L8S 4L7, Canada

4. Canadian Centre for Electron Microscopy, Hamilton, ON, L8S 4M1, Canada

5. School of Geography and Earth Sciences, McMaster University, Hamilton, ON, L8S 4K1, Canada; schwarcz@mcmaster.ca

Key words: transmission electron microscopy, EELS, collagen, apatite, ultramicrotome, ion milling, fibril, platelets, gap zone, HAADF.

Abstract

Transmission electron microscopic (TEM) images of ion-milled bovid cortical bone cut approximately normal to the axes of fibrils show that mineral occurs in the form of plates surrounding and laying between circular or elliptical features about 50 nm in diameter. The classification of these features as either pores or collagen fibrils is highly debated. Electron energy loss spectroscopy (EELS) mapping of these features in ion milled sections shows that they are lacking significant amounts of mineral or collagen, although their appearance suggests that they are cross sections of collagen fibrils. However, analogous sections prepared using an ultramicrotome show that, while these circular features show reduced concentrations of calcium and phosphorus, some of them contain quantities of carbon and nitrogen in bonding states comparable to the composition of collagen. This work demonstrates that the observed circular features are sections of collagen fibrils, but that bombardment by argon ions during broad beam ion milling destroys the collagen and associated gap-zone mineral.

1. Introduction

Bone is a composite material in which fibrils about 50 nm in diameter, bundles of triple helices of collagen, are spatially associated with an approximately equal volume of apatite mineral. The crystals of mineral are widely believed to occur inside gaps between the C and N termini of collinear collagen molecules inside the fibrils (Alexander et al., 2012; Landis and Song, 1991; McEwen et al., 1991; Weiner et al., 1991). In transmission electron microscopic (TEM) studies of ion-milled sections of bone we have shown, however, that most of the mineral in bone occurs

in the form of discrete, elongated, and plate-like mosaics of apatite crystals which surround and lie between the fibrils. We have previously described these plates as “mineral lamellae” (Grandfield et al., 2018; Schwarcz, 2015). In bone sections cut parallel to the long axis of long bones, the fibrils are recognizable by the presence of gap and overlap zones spaced every 67 nm along the fibril (Fig. 1). Mineral lamellae and fibrils can be seen in ion-milled and focused ion beam (FIB) sections of bone and dentine (Cressey and Cressey, 2003; Jantou-Morris et al., 2010; Jantou et al., 2009; McNally et al., 2012; Nalla et al., 2005; Srot et al., 2012; Tertuliano and Greer, 2016), but are not readily observable in ultramicrotome prepared sections of bone. This is believed to be a consequence of the diamond knife fracturing the brittle mineral lamellae (Jantou et al., 2009; McNally et al., 2012; Schwarcz, 2015; Srot et al., 2012).

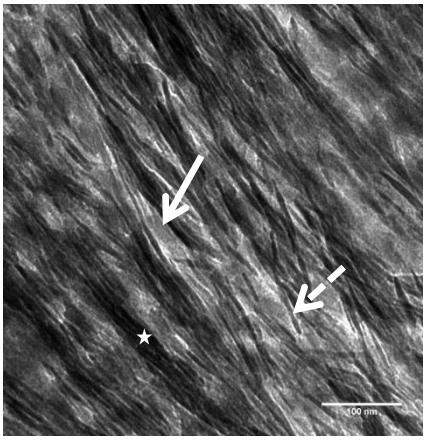

Fig. 1: Bright field transmission electron microscopy (BF-TEM) image of an ion milled section of bone cut parallel to the long axis of the femur of a mature cow. The characteristic gap-zone of collagen is readily observable along with what the authors define as a mineral lamellae. Solid arrow: gap-zone marked by higher electron density (darker); Dashed arrow: single mineral lamella; Star: stack of mineral lamellae, viewed edge-wise. Scale = 100 nm

When viewed in cross section, it is more difficult to identify the presence of collagen fibrils since the sections are cut normal to the distinctive gap/overlap zones and collagen itself has a low average atomic number leading to very low contrast in TEM images. However, all cross sections of cortical bone display a characteristic “lacy” appearance (Grandfield et al., 2018; McNally et al., 2012; Reznikov et al., 2014a) (Fig. 2). Mineral plates surround what appear to be holes which can appear circular, elliptical or irregular in shape. Some of the “holes” appear to be partially or completely filled with material which exhibits even lower electron contrast than the lowest-contrast areas of longitudinal sections. The “holes” are typically between 50 and 70 nm across, which is in agreement with known dimensions of collagen fibrils in bone (Katz and Li, 1973). Note that sections of the same bone sample, when viewed on a plane oriented at 90° to these sections, clearly display the presence of collagen fibrils (McNally *et al* ., 2012). Therefore, fibrils must be present somewhere in these cross sectional images and it seems possible that they were present in these circular features. McNally et al. (2012) suggest that the absence of material in

many of these features is due to erosion of the softer collagen by the beam of Ar^+ ions used to thin the section during broad beam ion milling. A similar proposal was made by Jantou et al. (2009) to account for the absence of material in holes observed in FIB sections of dentine and proposed that these features were sections of collagen fibrils. They noted that weakly electron-dense material was present in similar shaped features seen in ultramicrotome-cut sections of the same material. Conversely, Reznikov et al. (2014) have described the holes or circular features as devoid of material and are a consequence of viewing collagen from an oblique angle.

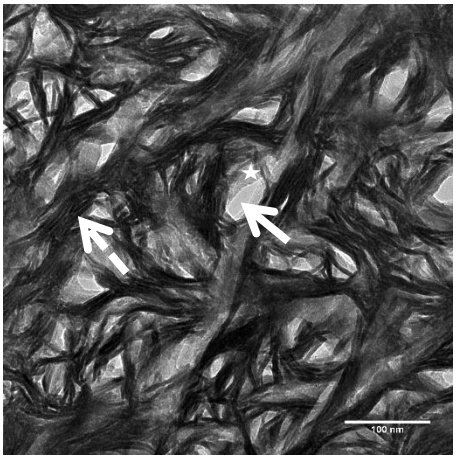

Fig. 2: BF-TEM image of an ion milled transverse section of a cow femur. Solid arrow: hole representing a possible site of collagen fibril; Dashed arrow: stack of multiple (~6) mineral lamellae, viewed edgewise; Star: lower electron density material, partially filling a hole. Scale = 100 nm

Here we attempt to demonstrate that these hole-like features are in fact cross-sections of collagen fibrils by analyzing the material in these features using electron energy loss spectroscopy (EELS). By evaluating the presence and bonding states of carbon and nitrogen in these features, we can determine whether collagen is present or not. EELS analyses have been carried out previously on bone sections cut parallel to the long axis and mineralized turkey tendon by Kłosowski *et al* (Kłosowski et al., 2018, 2017, 2015). They show spectra for C and N K-edges in bone and note the presence of discrete peaks which represent the bonding states characteristic of collagen. Wang *et al* . (Wang et al., 2018) also studied the C and N signals of bone with EELS in a correlative study of biomineralization.

In this study we proposed to test whether collagen was present in the circular features observed in bone sectioned normal to the long axis by mapping the intensity and spectral characteristics of the N and C K-edges.

2. Methods

2.1. Sample Preparation by Ion Milling

A section of the cortex of the femoral diaphysis of a mature cow (*Bos taurus*) was obtained from a frozen specimen. The sample was defatted in a 3:1 mixture of chloroform/methanol overnight and subsequently dehydrated in a graded series of ethanol. Sections were cut from this block perpendicular to the long axis of the femur so that the collagen fibrils would tend to be oriented normal to the plane of the section. Sections 1mm in thickness were cut using a water-cooled diamond wafering blade mounted in an IsoMet Low Speed Saw (Buehler). The sections were polished on both sides with 600 grit SiC papers to a final thickness of 100 μm. Discs (3 mm diameter) were cut from the 100 μm sections using a Gatan Model 601 ultrasonic disc cutter, and their centers were thinned to <50 μm with a Gatan Model 656 dimple grinder with 3 μm diamond paste. The discs were further dimpled to <30 μm with 1 μm diamond paste. Dimpled discs were then ion milled in a liquid nitrogen cooled Fischione 1010 ion mill until a hole was eroded in the sample. The ion mill stage was cooled to -75°C and rotated back and forth between -90° and +90°, with a 4 mA, 4 keV Ar^+ ion beam angled 4 to 6 degrees. A 5 nm coating of amorphous carbon was applied to the ion milled sections to reduce sample charging and heating in the electron microscope.

2.2. Sample Preparation by Ultramicrotomy

An identical section of cow bone was embedded in Spurr's epoxy resin under vacuum for several hours and then embedded in fresh resin and polymerized in a 60° C oven overnight. Thin sections (100 – 150 nm) were cut with a diamond knife on a Leica UCT ultramicrotome and picked up onto formvar-coated Cu grids. Some of the sections were post-stained with uranyl acetate.

The presence of a thin (~10nm) carbon coating on the ion-milled sections would contribute some uniform signal intensity to measurements of the carbon K-edge signal even in areas where no carbon was present in the sample. Additionally, the microtome-cut sections were mounted on a formvar-coated copper grid and this sample was embedded in Spurr's resin, both of which could contribute to the C K-edge signal uniformly across the entire sample. Therefore, significant point-to-point differences in the EELS C K-edge intensity and spectrum are due to the sample itself and not the grid or coating. EELS analysis of the resin showed that it did not contain detectable quantities of nitrogen, so even if present in the holes, it would not contribute a spurious N K-edge signal.

2.3. Transmission Electron Microscopy and EELS

BF-TEM images of all the sections were obtained on a Phillips CM12 electron microscope operated at 120 kV. Electron energy loss spectroscopy (EELS) and high-angle annular dark-field (HAADF) images were obtained using a JEOL 2010F electron microscope equipped with a Gatan Imaging Filtering (GIF) system (Gatan Inc., Pleasanton, CA, USA) operated at 200 kV.

EELS spectrum images were collected in STEM mode at 200kV with 1 nm electron probe size with a convergence semi-angle of 10 mrad and collection semi-angle was 30 mrad. Energy resolution defined by full width at half maximum (FWHM) was 1-1.2 eV using an energy dispersion of 0.3 eV/channel. The acquisition time for spectra was 0.1s. In order to keep the acquisition short, pixel size varied from 2 to 4 nm.

Digital Micrograph (Gatan Inc., Pleasanton, CA, USA) was used for EELS analysis. Spectra were background subtracted and processed using principal component analysis (PCA). The bonding of specific elements was determined using energy-loss near-edge structure (ELNES). Colour maps were generated from elemental composition and excluded ELNES from the quantification.

3. Results

3.1 EELS spectra of ion-milled sections

HAADF images of a section cut using the ion mill resembled that shown in Fig 2. Individual mineral lamellae surround the circular or elliptical regions (“holes”) in which only patches of weakly electron-scattering material can be seen. The remainder of these hole-like features appears to be empty. One such hole is shown in a map of Ca abundance for one of these holes (Fig 3), from which we have obtained representative EELS spectra for the C, N, Ca, and P edges.

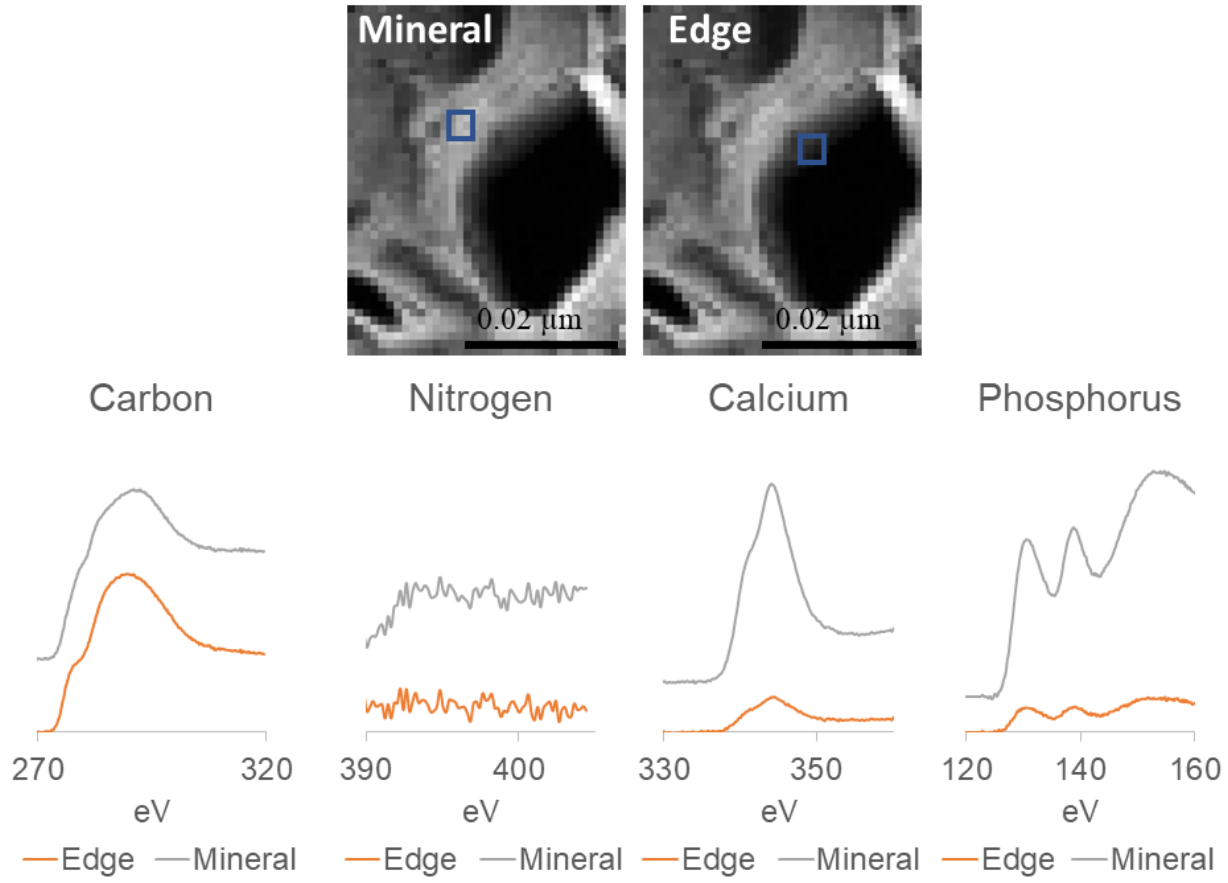

Fig. 3. EELS spectrum images of a single hole-like feature in a cross section of cow bone prepared by ion milling, showing the EELS edge spectra for C, N, Ca and P, as recorded at two positions on the image: at the edge of the hole ("Edge"), and in the mineral matrix surrounding the hole ("Mineral"). The y-axis is arbitrary units and represents only relative intensities of signals.

The Ca and P signals are present in both areas, but are relatively stronger in the mineral compared to the edge of the hole. It was not possible to obtain signal for any element within the hole as it was devoid of any signal. The observed spectra for Ca and P resemble the Ca L_{2-3} and P L_{2-3} edges shown in Kłosowski et al. (2017, Supplemental Material). The carbon signal is effectively identical both in terms of bonding and intensity within the mineral and at the edge. This C edge resembles the energy-loss near-edge structure (ELNES) shown by Kłosowski et al. (2017, Supplemental Material) but is much less well resolved. There is minimal to no detection of nitrogen in the sample both at the mineral and edge sampling regions. When examined extremely precisely, a singular peak of nitrogen can be observed in the mineral region only. This peak shape appears to be similar to that of elemental nitrogen but the energy resolution of this data limits the capacity of the authors to properly characterize it.

The result that no signal is detected within the hole agrees with previous observations that cross sections of fibrils in ion milled sections are too severely eroded by the ion beam to permit

conclusive testing. Therefore, despite the risk of damage to the mineral lamellae, ultramicrotome-cut sections were prepared in an attempt to avoid ion-beam erosion of the collagen fibrils.

3.2 EELS spectra of microtome-cut sections

While collagen should be still present in microtome-cut sections, TEM images of such sections show (Jantou et al., 2009; McNally et al., 2012; Schwarcz, 2015; Srot et al., 2012) that many structural features of the bone are seriously damaged by the action of the diamond blade. As a result, HAADF images of microtomed sections often lack well-defined mineral lamellae. Nevertheless, it is still possible to identify in this section cut normal to the long axis of the femur, the presence of hole-like features. Many of the holes in the microtome-cut section were empty or contained only residual patches of weakly electron-dense material. However, a few holes were largely or completely filled with this material, and the EELS spectrum for one of them is shown in Fig. 4.

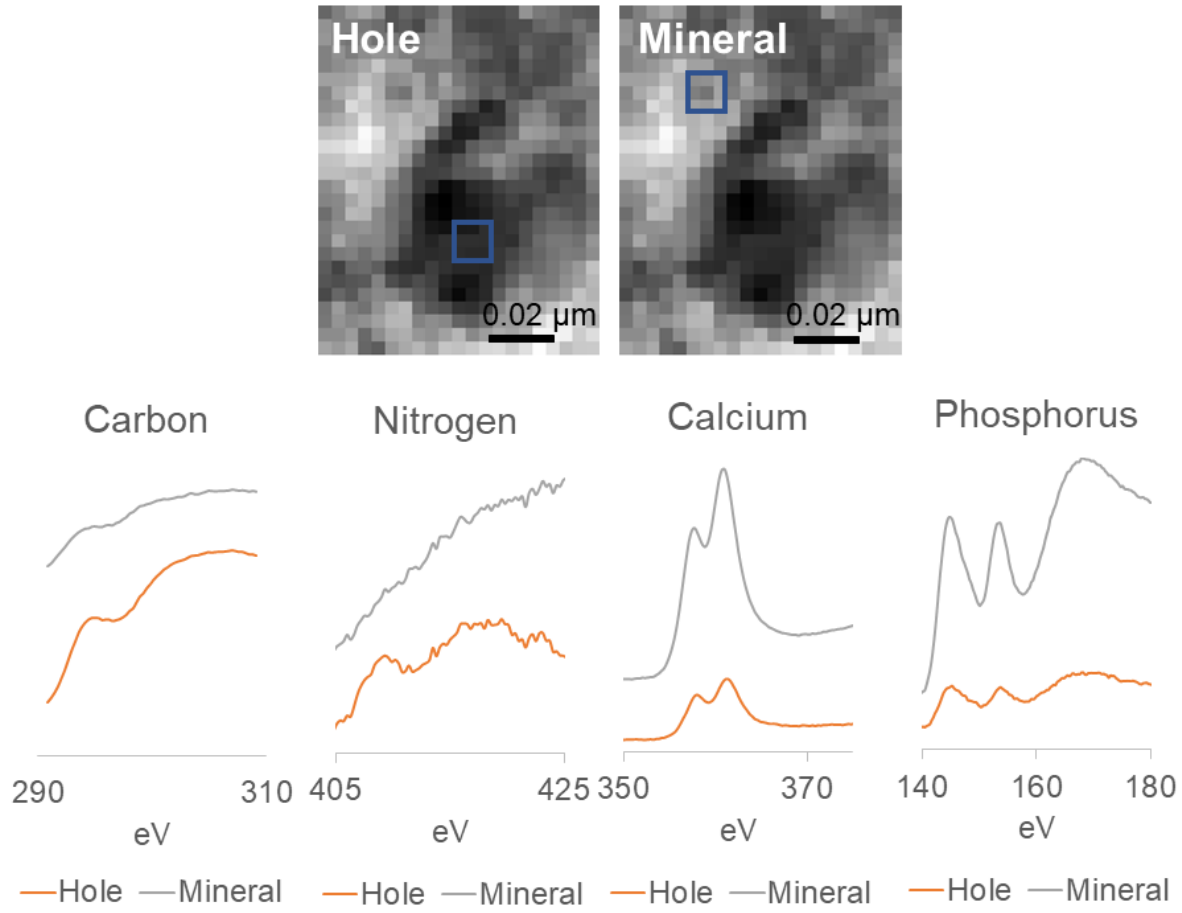

Fig. 4. EELS spectrum images of microtome-cut section of cow bone and EELS spectra for C, N, Ca and P from selected locations: outside hole ("Mineral") and inside hole ("Hole"). The y-axis is arbitrary units and represents only relative intensities of signals.

The EELS spectra for Ca and P and for C in the mineral outside the hole are similar to those for the ion milled section. The relative intensities of Ca and P are again greater in the mineralized region compared to in the hole, but are nevertheless still present in the same bonding states in both locations. For carbon, there is a relative increase in signal intensity in the hole region compared to the mineral region, suggesting an additional contribution to the signal above the background formvar grid. There is a very minor peak in the shoulder following the initial primary peak which has been attributed to aromatic groups or from collagen crosslinking (Bhattacharyya et al., 2002; Leinweber et al., 2007). The broad peak following the initial peak and shoulder is attributed to carbonate bonding. Similar carbon structures were also shown by Kłosowski et al.(2017, Supporting Information). Unlike with the ion-milled sample, there are well-defined nitrogen peaks in the microtomed section. The bonding structure appears different in the mineral region compared to the hole region. The presence of two distinct nitrogen peaks, similar to the observations in the carbon edge, can be considered contribution from aromatic rings or collagen (Bhattacharyya et al., 2002; Leinweber et al., 2007). Additionally, other authors

have shown that specific amino acids such as glycine and proline, both involved in collagen structure, have dual broad peaks (Plekan et al. (2007)) and these peaks could potentially be attributed to these amino acids as well.

3.3 Comparative maps of element abundance

To provide additional evidence on whether or not collagen was present in the holes of the sectioned bone, EELS maps showing the relative abundance of the four elements for which we had collected spectral data were collected. These are shown in Fig 5, which also shows corresponding HAADF images. As was mentioned previously, there is a lack of recognizable mineral lamellae in the HAADF image of the microtome-cut sample.

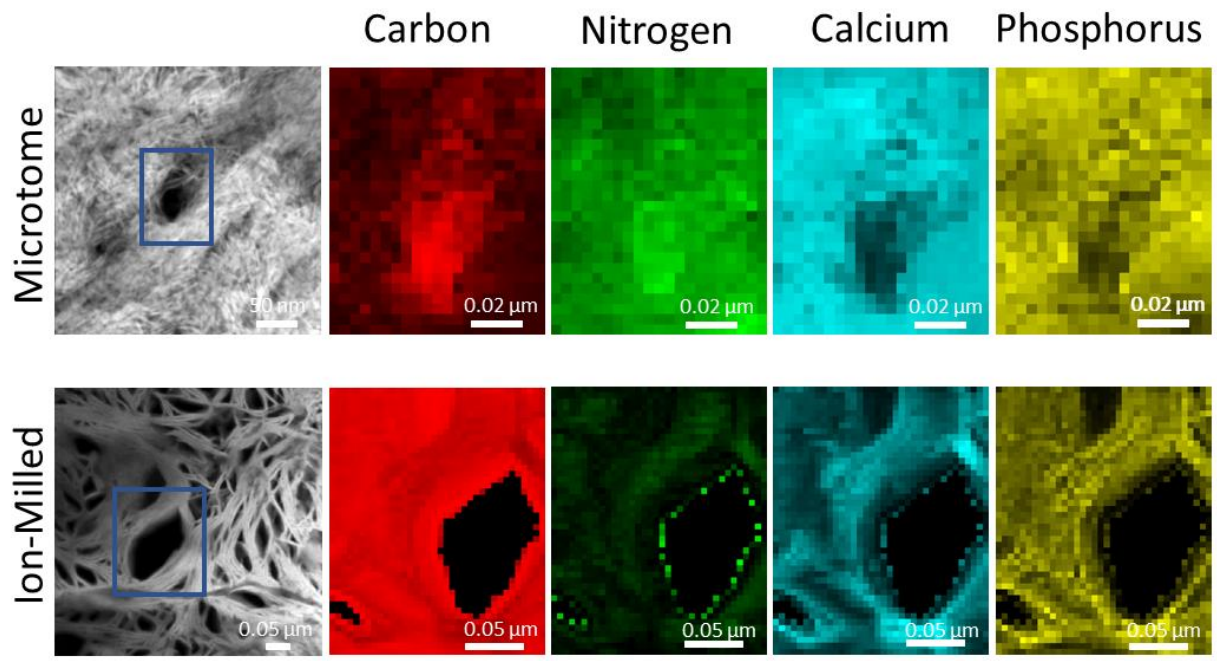

Fig. 5. HAADF images of ion milled and microtome cut sections of cow bone, together with EELS maps of relative intensities of for C, N, Ca and P. It is clear that stronger C and N signals are present in the hole of the microtomed section, likely representing collagen.

The figure shows that significantly higher concentrations of both carbon and nitrogen are present in the hole of the microtome-cut section, compared with the levels outside the hole. This is consistent with spectral analysis. The relative intensity of the Ca and P EELS signals in the holes is less than the surrounding region but both Ca and P are still very evident in the hole.

In contrast, the hole shown in the ion milled section is devoid of any of the elements for which we measured EELS intensity. The surrounding area shows a high carbon content which can be partly attributed to the carbon coating as well as other sample preparation methods. This is consistent with previous observations that the ion beam milling process selectively removes collagen from these holes.

4. Discussion

TEM images of ion-milled sections of cortical bone cut normal to the axes of collagen fibrils typically display open regions which appear to be holes in the section. The content of these holes is debated within the bone structure community. This work shows, via EELS spectra in microtome-cut sections, that the contents of the holes appear to have carbon and nitrogen constituents consistent with characteristic EELS peaks for collagen, which suggests that there is indeed collagen present in these holes. It follows that this material could be assumed to be collagen as this is the most abundant organic material in bone. The disadvantage of using such sections is that the diamond knife used to cut them causes significant damage to the structure of bone (McNally et al., 2012; Schwarcz, 2015), leading to breakage of the relatively brittle mineral lamellae into small fragments. However, in sections cut normal to the axes of collagen fibrils, the

circular form of these fibrils can still be detected (McNally et al., 2012; Rubin et al., 2003). Nevertheless, we noted that many of the holes in the microtome-cut sections were also either empty or only partially filled with organic material.

These data show that the holes identified in cross sections of bone may not be as empty as has been claimed by some authors (Reznikov et al., 2014a)). The findings of our work are more in line with what was first suggested by Jantou et al.,(2009) who state that these circular or elliptical features appear to be cross sections of collagen fibrils. Subsequent work has suggested that the collagen fibrils tend to be eroded away by the ion beam in both ion and focused ion beam milling sample preparation (McNally et al., 2012; Grandfield et al., 2018). A complicating and unavoidable factor is of course bone sample preparation, which often involves fixation, staining, dehydration, and embedding. In this work we attempted to limit sample processing to dehydration, embedding and post-staining, the effects of which we can safely identify via elemental analysis.

The hypothesis that these circular structures represent collagen fibrils is not particularly outlandish when one considers other independent evidence. First, it is well known that collagen constitutes about 25 wt% of bone (Arnold et al. 2001) which, due to the lower density of collagen compared to mineral, corresponds to about 50 volume percent. This logic suggests that in any section of bone a substantial area should be occupied by collagen fibrils; in the cross sectional views shown here it is apparent that the only place where these could be located would be in the hole-like structures. Reznikov *et al*. (2014b) argue that the holes seen in the images shown by Cressey and Cressey (2003) and McNally et al. (2012) would only be found in what they refer to as disordered material, rather than ordered, normal bone. However, in every section which we have made, where the plane of the section is normal to the fibril axes, we have seen holes like those discussed in this paper (e.g., Grandfield et al., 2018)). While it is possible that every section of bone the authors have prepared was fortuitously of disordered material, it is unlikely that all these randomly positioned sections were of disordered bone, which makes up only a few percent of bone (Reznikov *et al* ., 2014).

5. Conclusions

Elemental analysis is a key component to understanding the ultrastructural organization of bone. By sectioning bovine bone normal to its long axis we were able to observe hole-like features that EELS analysis suggests are indeed collagen fibrils. Specifically, the presence and chemical bonding of nitrogen in these regions is consistent with collagen. This work has also identified that the method of preparing bone sections has a drastic influence on the interpretation of bone ultrastructure, where ion milled sections are completely devoid of material in these holes while ultramicrotomy disrupts mineral. A careful optimization of bone sample preparation for TEM that maintains collagen and mineral may be possible by focused ion beam methods.

Acknowledgements

This research was funded by a grant to HPS from the Natural Sciences and Engineering Research Council of Canada (NSERC). Microscopy was conducted at the Canadian Centre for Electron Microscopy. None of the authors have any financial commitments arising from this study.

References

Alexander, B., Daulton, T.L., Genin, G.M., Lipner, J., Pasteris, J.D., Wopenka, B., Thomopoulos, S., 2012. The nanometre-scale physiology of bone: steric modelling and scanning transmission electron microscopy of collagen-mineral structure. J. R. Soc. Interface 9, 1774–1786. https://doi.org/10.1098/rsif.2011.0880

Arnold, S., Plate, U., Wiesmann, H.P., Stratmann, U., Kohl, H., Höhling, H.J., 2001. Quantitative analyses of the biomineralization of different hard tissues. J. Microsc. 202, 488–494. https://doi.org/10.1046/j.1365-2818.2001.00831.x

Bhattacharyya, S., Lubbe, M., Bressler, P.R., Zahn, D.R.T., Richter, F., 2002. Structure of nitrogenated amorphous carbon films from NEXAFS. Diam. Relat. Mater. 11, 8–15. https://doi.org/https://doi.org/10.1016/S0925-9635(01)00525-8

Cressey, B.A., Cressey, G., 2003. A model for the composite nanostructure of bone suggested by high-resolution transmission electron microscopy. Mineral. Mag. 67, 1171–1182. https://doi.org/10.1180/0026461036760156

Grandfield, K., Vuong, V., Schwarcz, H.P., 2018. Ultrastructure of Bone : Hierarchical Features from Nanometer to Micrometer Scale Revealed in Focused Ion Beam Sections in the TEM. Calcif. Tissue Int. 103, 606–616. https://doi.org/10.1007/s00223-018-0454-9

Jantou-Morris, V., Horton, M.A., McComb, D.W., 2010. The nano-morphological relationships between apatite crystals and collagen fibrils in ivory dentine. Biomaterials 31, 5275–5286. https://doi.org/10.1016/j.biomaterials.2010.03.025

Jantou, V., Turmaine, M., West, G.D., Horton, M.A., McComb, D.W., 2009. Focused ion beam milling and ultramicrotomy of mineralised ivory dentine for analytical transmission electron microscopy. Micron 40, 495–501. https://doi.org/10.1016/j.micron.2008.12.002

Katz, E.P., Li, H., 1973. Structure and Function of Bone Collagen Fibrils. J.Mol.Bio. 80, 1–15. https://doi.org/https://doi-org.libaccess.lib.mcmaster.ca/10.1016/0022-2836(73)90230-1

Kłosowski, M.M., Abellan, P., Ramasse, Q., Mccomb, D.W., Porter, A.E., Shefelbine, S.J., 2017. Electron Microscopy Reveals Structural and Chemical Changes at the Nanometer Scale in the Osteogenesis Imperfecta Murine Pathology 2788–2797. https://doi.org/10.1021/acsbiomaterials.6b00300

Kłosowski, M.M., Carzaniga, R., Shefelbine, S.J., Porter, A.E., Mccomb, D.W., 2018. Nanoanalytical electron microscopy of events predisposing to mineralisation of turkey tendon 1–11. https://doi.org/10.1038/s41598-018-20072-2

Kłosowski, M.M., Friederichs, R.J., Nichol, R., Antolin, N., Carzaniga, R., Windl, W., Best, S.M., Shefelbine, S.J., Mccomb, D.W., Porter, A.E., 2015. Acta Biomaterialia Probing carbonate in bone forming minerals on the nanometre scale 20, 129–139. https://doi.org/10.1016/j.actbio.2015.03.039

Landis, W.J., Song, M.J., 1991. Early mineral deposition in calcifying tendon characterized by high voltage electron microscopy and three-dimensional graphic imaging. J. Struct. Biol. 107, 116–127. https://doi.org/10.1016/1047-8477(91)90015-O

Leinweber, P., Kruse, J., Walley, F.L., Gillespie, A., Eckhardt, K., Blyth, I.R., Regier, T., 2007. Nitrogen K -edge XANES – an overview of reference compounds used to identify " unknown " organic nitrogen in environmental samples. J. Synchrot. Radiat. 500–511. https://doi.org/10.1107/S0909049507042513

McEwen, B.F., Song, M.J., Landis, W.J., 1991. Quantitative determination of the mineral distribution in different collagen zones of calcifying tendon using high voltage electron microscopic tomography. J. Comput. Assist. Microsc. 3, 201–10.

McNally, E.A., Schwarcz, H.P., Botton, G.A., Arsenault, A.L., 2012. A model for the ultrastructure of bone based on electron microscopy of ion-milled sections. PLoS One. https://doi.org/10.1371/journal.pone.0029258

Nalla, R.K., Porter, A.E., Daraio, C., Minor, A., Radmilovic, V., Stach, E., Tomsia, A., Ritchie,

R., 2005. Ultrastructural examination of dentin using focused ion-beam cross-sectioning and transmission electron microscopy. Micron 36, 672–680. https://doi.org/https://doi.org/10.1016/j.micron.2005.05.011

Plekan, O., Feyer, V., Richter, R., Coreno, M., de Simone, M., Prince, K.C., Carravetta, V., 2007. An X-ray absorption study of glycine, methionine and proline. J. Electron Spectros. Relat. Phenomena. https://doi.org/10.1016/j.elspec.2006.11.004

Reznikov, N., Shahar, R., Weiner, S., 2014a. Three-dimensional structure of human lamellar bone: The presence of two different materials and new insights into the hierarchical organization. Bone 59, 93–104. https://doi.org/10.1016/j.bone.2013.10.023

Reznikov, N., Shahar, R., Weiner, S., 2014b. Bone Hierarchical Structure in 3 Dimensions. Acta Biomater. 10, 3815–3826. https://doi.org/10.1016/j.actbio.2014.05.024

Rubin, M.A., Jasiuk, I., Taylor, J., Rubin, J., Ganey, T., Apkarian, R.P., 2003. TEM analysis of the nanostructure of normal and osteoporotic human trabecular bone. Bone 33, 270–282. https://doi.org/10.1016/S8756-3282(03)00194-7

Schwarcz, H.P., 2015. The ultrastructure of bone as revealed in electron microscopy of ion-milled sections. Semin. Cell Dev. Biol. 46. https://doi.org/10.1016/j.semcdb.2015.06.008

Schwarcz, H.P., 2015. The ultrastructure of bone as revealed in electron microscopy of ion-milled sections. Semin. Cell Dev. Biol. 46, 44–50. https://doi.org/10.1016/j.semcdb.2015.06.008

Srot, V., Bussmann, B., Salzberger, U., Koch, C.T., van Aken, P.A., 2012. Linking Microstructure and Nanochemistry in Human Dental Tissues. Microsc. Microanal. 18, 509–523. https://doi.org/doi:10.1017/S1431927612000116

Tertuliano, O.A., Greer, J.R., 2016. The nanocomposite nature of bone drives its strength and damage resistance. Nat. Mater. 15, 1195–1202. https://doi.org/10.1038/nmat4719

Wang, X., Langelier, B., Shah, F.A., Korinek, A., Bugnet, M., Hitchcock, A.P., Palmquist, A., Grandfield, K., 2018. Biomineralization at Titanium Revealed by Correlative 4D Tomographic and Spectroscopic Methods. Adv. Mater. Interfaces.

https://doi.org/10.1002/admi.201800262

Weiner, S., Arad, T., Traub, W., 1991. Crystal organization in rat bone lamellae. FEBS Lett. 285, 49–54. https://doi.org/10.1016/0014-5793(91)80722-F